Floquet Engineering of Two Weakly Coupled Superconducting Flux Qubits

Wan-Lu Song (宋婉露)[1,2] Jia-Bin You (游佳斌),[3] J.K. Xu (徐家坤),[4,*] W.L. Yang (杨万里),[2,†] and Jun-Hong An (安钧鸿)[5]

[1] *Department of Physics, Hubei University, Wuhan 430062, China*
[2] *State Key Laboratory of Magnetic Resonance and Atomic and Molecular Physics, Innovation Academy for Precision Measurement Science and Technology, Chinese Academy of Sciences, Wuhan 430071, China*
[3] *Department of Electronics and Photonics, Institute of High Performance Computing, 1 Fusionopolis Way, 16-16 Connexis, Singapore 138632, Singapore*
[4] *School of Electronics and Electrical Engineering, Wuhan Textile University, Wuhan 430200, China*
[5] *School of Physical Science and Technology, Lanzhou University, Lanzhou 730000, China*

(Received 15 April 2020; accepted 13 October 2020; published 19 November 2020)

We explore the periodically driven dynamics of two weakly coupled flux qubits and propose a scheme to generate a maximally entangled state based on Floquet engineering. The periodic driving modifies the quasienergy spectrum of the system and induces crossing of quasienergies, and the weak coupling between them lifts the degeneracy of quasienergies. It is found that the phenomena of entanglement resonance of Floquet state appear at certain values of the driving parameters, which could be demonstrated by virtue of the Rabi-frequency spectrum and average concurrence during one driving period. Our scheme relaxes the experimental difficulty in adjusting the static parameters of the system to establish entanglement, and may open interesting perspectives for devising active decoherence-immune quantum-information devices.

DOI: 10.1103/PhysRevApplied.14.054049

I. INTRODUCTION

Recently, strong periodic driving has played a profound role in the research field about coherent quantum dynamics and quantum many-body system [1–13]. Various nontrivial effects along with a wealth of new quantum phenomena have been discovered successively in periodically driven or Floquet systems [14–24,24–34]. Other theoretical progress includes the generic relaxation problem [35], the theory of Floquet time crystals [36], the renormalization problem [37], dynamical freezing [38], synchronization [17], and strong-coupling theory [39]. Experimentally, series of interesting phenomena including many-body localization [40], unprecedented dynamics of Rydberg atoms [11], discrete time crystals in trapped ions [41], nuclear magnetic resonance systems [42,43], and nitrogen-vacancy centers [44], have been found in succession.

Controlling the quasienergy spectrum of periodically driven systems could bring more abundant quasistationary-state behaviors than the static case. It provides the possibility of controlling the complex coherent dynamics of microscopic systems and generating alternative nonequilibrium quantum states absent in the original static system [45–47]. Additionally, the dynamics governed by Rabi oscillations and the commonly used rotating wave approximation (RWA) [48] in the weak driving case breaks down, when the system is driven strongly with the Rabi frequency comparable to the relevant transition frequency. It results in complex evolution dominated also by counterrotating wave, which could be adequately described in the framework of Floquet theory [49,50]. On the other hand, the superconducting flux qubits offer various prospects to study quantum-information processing owing to their eminent properties [51–68]. Recently, Floquet states in a single flux qubit have been observed using quantum-state tomography and strongly driven microwave pulses with controllable shape [69], which pave the way to quantum control and quantum simulation using periodically strong driving with applications in circuit QED [12].

Inspired by these experimental and theoretical developments, we investigate the Floquet dynamics of two weakly coupled flux qubits under strong periodic driving with different conditions. Here the Floquet equation can be solved in the Sambe space [70,71] using the generalized Van Vleck nearly degenerate perturbation theory [72,73]. We also explore the realization of maximally entangled Floquet state of flux qubits based on the technique of Floquet engineering. Through modifying the quasienergy spectrum by strong periodic driving, we find that the appearance of crossing levels in the quasienergy spectrum at certain

*xujiakun@wtu.edu.cn
†ywl@wipm.ac.cn

values of the driving parameters. We further reveal that the presence of weak coupling between flux qubits lifts the degeneracy of quasienergies and induces the entanglement resonance of Floquet state. This phenomenon can be verified by the behaviors of the quasienergy spectrum and time-average entanglement of Floquet states characterized by the average concurrence during one driving period. Also, the signature of entanglement resonance could be figured out when the degeneracy of quasienergies disappears, from the Rabi-frequency spectrum through Fourier transform of the time-dependent population signal. Our method suggests that the entanglement protection can be realized by suppressing decoherence in a temporal domain, when the system is initialized into a maximally entangled Floquet state. This critical result can be used for devising active decoherence-immune quantum-information devices.

The remainder of this paper is organized as follows. In Sec. II, we describe the periodically driven system and its theoretical framework. In Sec. III, the Rabi-frequency spectrum by Fourier transform of the time-dependent population signal is investigated. In Sec. IV, we explore the behaviors of Floquet spectrum and time-average entanglement of Floquet states under different driving conditions. The scheme to initialize the system into one maximally entangled Floquet state is presented in Sec. V. In Sec. VI, we discuss the experimental feasibility of the proposed scheme and make a conclusion.

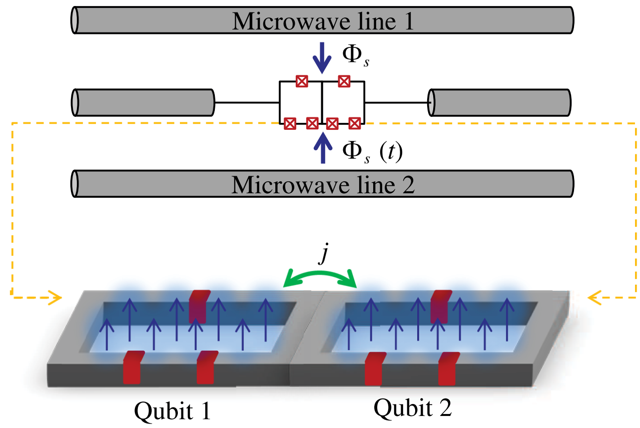

FIG. 1. Schematic representation of two weak coupling flux qubits, each of which is formed by three Josephson junctions (red cross) interrupting a superconducting loop with the enlarged image shown below. The two flux qubits are coupled by the mutual indutance J (green arrow); two microwave lines are applied to provide a static magnetic flux Φ_s and a time-periodically varying magnetic flux $\Phi_d\,(t)$ through the loops of both flux qubits (blue arrow), respectively.

II. MODEL

As shown in Fig. 1,two flux qubits are weakly coupled by sharing one side of a superconducting loop. Besides, there are two microwave lines providing static magnetic flux Φ_s and time-periodically varying magnetic flux $\Phi_d\,(t) = |\Phi_d|\cos(\omega t)$ through both loops. Thus, the total Hamiltonian of this system can be written as

$$\hat{H}\,(t) = \sum_{j=1,2}\left[\frac{1}{2}\left(\varepsilon\hat{\sigma}_j^z + \Delta\hat{\sigma}_j^x\right) + \Omega\cos(\omega t)\,\hat{\sigma}_j^z\right] + J\hat{\sigma}_1^z\hat{\sigma}_2^z, \tag{1}$$

where $\hat{\sigma}_j^x$ and $\hat{\sigma}_j^z$ are Pauli operators of the jth flux qubits. $\varepsilon = 2I_p\,(\Phi_s - \Phi_0/2)$ is the energy-level separation and Δ is the tunneling energy between clockwise and anticlockwise circulating classical states ($|0\rangle$ and $|1\rangle$) of persistent current I_p, where Φ_0 is the flux quantum [51]. In our scheme, the energy degeneracy point $\varepsilon = 0$ is considered. $\Omega = I_p\,|\Phi_d|$ is the driving strength. $J = MI_{p1}I_{p2}$ is the inductively coupling strength, where M is the coefficient of mutual induction [53,57].

For a time-periodic Hamiltonian $\hat{H}\,(t) = \hat{H}\,(t+T)$ with $T = 2\pi/\omega$, any solution of the related Schrödinger equation $i\partial_t\,|\Psi\,(t)\rangle = \hat{H}\,(t)\,|\Psi\,(t)\rangle$ can be decomposed by a superposition of an orthogonal and complete set of basis $\{|u_r\,(t)\rangle\}$ as $|\Psi\,(t)\rangle = \sum_r a_r e^{-i\epsilon_r t}\,|u_r\,(t)\rangle$. a_r is the time-independent weighting factors of the superposition. ϵ_r and $|u_r\,(t)\rangle$ are called quasienergies and Floquet states (quasienergy states), governed by the Floquet equation

$$\hat{H}_F\,|u_r\,(t)\rangle = \epsilon_r\,|u_r\,(t)\rangle\,. \tag{2}$$

$\hat{H}_F = \hat{H}\,(t) - i\partial_t$ is the Floquet Hamiltonian.

According to the Fourier transform, the time-periodic Floquet state $|u_r\,(t)\rangle$ can be expanded by a complete set of basis vectors $\left\{e^{ik\omega t}|k\in\mathbb{Z}\right\}$ in the temporal space as

$$|u_r\,(t)\rangle = \sum_k \left|\tilde{u}_{r,k}\right\rangle e^{ik\omega t}, \tag{3}$$

with $\left|\tilde{u}_{r,k}\right\rangle = 1/T\int_0^T |u_r\,(t)\rangle\,e^{-ik\omega t}dt$. In the Sambe space made up of the Hilbert space and the temporal space [70,71], the so-called Floquet matrix can be written as

$$\hat{H}_F = \begin{pmatrix} \ddots & & & & & & \\ & \hat{H}_0^{(-2)} & \hat{H}_1 & 0 & 0 & 0 & \\ & \hat{H}_1 & \hat{H}_0^{(-1)} & \hat{H}_1 & 0 & 0 & \\ & 0 & \hat{H}_1 & \hat{H}_0^{(0)} & \hat{H}_1 & 0 & \\ & 0 & 0 & \hat{H}_1 & \hat{H}_0^{(1)} & \hat{H}_1 & \\ & 0 & 0 & 0 & \hat{H}_1 & \hat{H}_0^{(2)} & \\ & & & & & & \ddots \end{pmatrix}, \tag{4}$$

with $\hat{H}_0^{(k)} = \sum_{j=1,2} (\Delta/2)\,\hat{\sigma}_j^x + J\hat{\sigma}_1^z\hat{\sigma}_2^z + k\omega$, $\hat{H}_1 = \sum_{j=1,2} (\Omega/2)\,\hat{\sigma}_j^z$. Truncating the basis vectors of the temporal space at $e^{\pm iN\omega t}$ with the convergence being guaranteed, the quasienergies $\epsilon_r + n\omega$ and Floquet states $e^{in\omega t}\,|u_r(t)\rangle$ in the Floquet zone $[n\omega, n\omega+\omega)$ can be obtained, where n is an integer between $-N$ and N. In each zone, there are quadruplet quasienergies and Floquet states, which can fully determine the properties of the periodic driving system.

III. WITNESS OF QUASIENERGY SPECTRUM

Since the quasienergies determine the inherent Rabi frequencies featured in the Floquet system, the Fourier transform of time-dependent dynamics is an efficient way to witness the quasienergy spectrum in experiment. Specifically speaking, the Fourier expansion of an operator's expectation $\langle\Psi(t)|\,\hat{O}\,|\Psi(t)\rangle$ in the Floquet system can be written as $\sum_{r,r',k,k'} a_r a_{r'} e^{i[(\epsilon_r-\epsilon_{r'})+(k'-k)\omega]t}\left\langle\tilde{u}_{r,k}\right|\hat{O}\left|\tilde{u}_{r',k'}\right\rangle$. Thus, the various frequency components shown in dynamical oscillations are determined by $\pm\epsilon_R + n\omega$, with $\epsilon_R = \epsilon_r - \epsilon_{r'}$ the quasienergy difference and $n = k' - k$ the integer values. As the periodic driving field has the additional symmetry $\cos[\omega(t+T/2)] = -\cos(\omega t)$, only components with even n are present.

Here, we focus on the dynamics of population in the doubly excited state $|11\rangle$ as shown in Figs. 2(a) and 2(b). Inthe weak driving regime $\Omega/\Delta \ll 1$ [Fig. 2(a)], the population is analogous to the Rabi oscillation predicted based on the RWA. However, in the strong driving regime [Fig. 2(b)], Rabi oscillation disappears due to the counterrotating wave. Making the Fourier transform on population dynamics under different conditions, inherent Rabi frequencies of the system are drawn in Figs. 2(c) and 2(d). For a certain value of J, the bright lines representing the frequency components have translational symmetry with the period 2ω ($\omega = \Delta$ for the resonant case). It is valid in strong driving regime and disappears in weak driving regime. There are more frequency components springing out than the case of Floquet engineering on a single flux qubit [69]. Besides, slightly splitting of the bright lines occurs due to the weak coupling between two qubits.

To clarify the frequency components presented above, we solve the Floquet equation by using the generalized Van Vleck nearly degenerate perturbation theory [72,73] (see more details in Appendix A). In the limit of $\Delta \ll \Omega$ and $J \ll \omega$, the Floquet matrix can be reduced into a 4×4 effective matrix

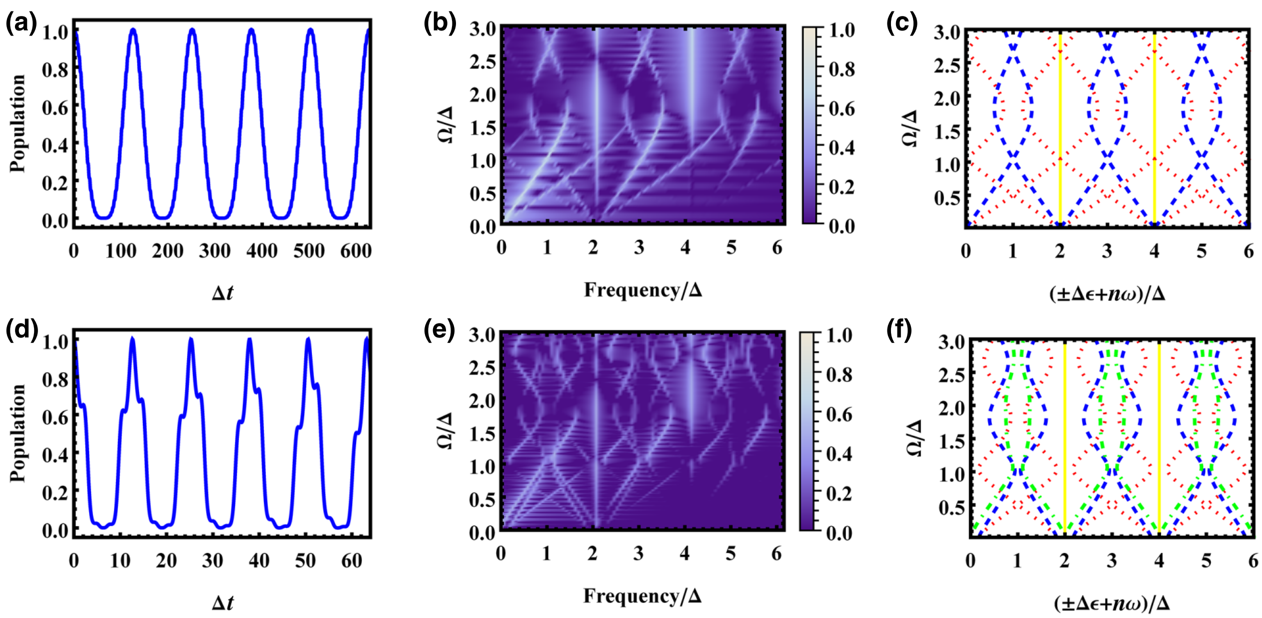

FIG. 2. Population dynamics and Rabi frequencies of the two qubits driven on resonant ($\omega = \Delta$) are studied for different driving strengths and coupling strengths defined in terms of Δ. Average population of the doubly excited state $|11\rangle$ versus time for $\Omega/\Delta = 0.05$ in (a) and $\Omega/\Delta = 0.5$ in (b) with $J = 0$. Density plot of the Fourier transform of population oscillations versus driving strength for $J = 0$ in (c) and $J/\Delta = 0.2$ in (d). Difference of quasienergies based on Floquet theory versus driving strength for $J = 0$ in (e) and $J/\Delta = 0.2$ in (f).

$$\hat{H}_{\mathrm{GVV}}=\begin{pmatrix} J+\varkappa\Delta^2\tilde{\mathcal{J}}_1^2 & \frac{1}{2}\Delta\tilde{\mathcal{J}}_0 & \frac{1}{2}\Delta\tilde{\mathcal{J}}_0 & -\varkappa\Delta^2\tilde{\mathcal{J}}_1^2 \\ \frac{1}{2}\Delta\tilde{\mathcal{J}}_0 & -J-\varkappa\Delta^2\tilde{\mathcal{J}}_1^2 & -\varkappa\Delta^2\tilde{\mathcal{J}}_1^2 & \frac{1}{2}\Delta\tilde{\mathcal{J}}_0 \\ \frac{1}{2}\Delta\tilde{\mathcal{J}}_0 & -\varkappa\Delta^2\tilde{\mathcal{J}}_1^2 & -J-\varkappa\Delta^2\tilde{\mathcal{J}}_1^2 & \frac{1}{2}\Delta\tilde{\mathcal{J}}_0 \\ -\varkappa\Delta^2\tilde{\mathcal{J}}_1^2 & \frac{1}{2}\Delta\tilde{\mathcal{J}}_0 & \frac{1}{2}\Delta\tilde{\mathcal{J}}_0 & J+\varkappa\Delta^2\tilde{\mathcal{J}}_1^2 \end{pmatrix}, \tag{5}$$

where $\varkappa = 2J/(4J^2-\omega^2)$, $\tilde{\mathcal{J}}_n = \mathcal{J}_n(2\Omega/\omega)$ with $\mathcal{J}_n$ the Bessel function. By solving the eigenequation of $\hat{H}_{\mathrm{GVV}}$, one can obtain the four quasienergies in one Floquet zone

$$\epsilon_1 = -J, \tag{6}$$

$$\epsilon_2 = J + 2\varkappa\Delta^2\tilde{\mathcal{J}}_1^2, \tag{7}$$

$$\epsilon_3 = -\varkappa\Delta^2\tilde{\mathcal{J}}_1^2 - \sqrt{\Delta^2\tilde{\mathcal{J}}_0^2 + \left(J+\varkappa\Delta^2\tilde{\mathcal{J}}_1^2\right)^2}, \tag{8}$$

$$\epsilon_4 = -\varkappa\Delta^2\tilde{\mathcal{J}}_1^2 + \sqrt{\Delta^2\tilde{\mathcal{J}}_0^2 + \left(J+\varkappa\Delta^2\tilde{\mathcal{J}}_1^2\right)^2}. \tag{9}$$

According to the identity principle, the Floquet state of the time-periodic system is either symmetric or antisymmetric under the exchange of the qubits. For two qubits, the antisymmetric subspace only consists of the singlet state $(|\uparrow\downarrow\rangle - |\downarrow\uparrow\rangle)/\sqrt{2}$. However, the symmetric subspace is spanned by triplet states $|\uparrow\uparrow\rangle$, $|\downarrow\downarrow\rangle$, and $(|\uparrow\downarrow\rangle + |\downarrow\uparrow\rangle)/\sqrt{2}$ [$|\uparrow\rangle = (|0\rangle+|1\rangle)/\sqrt{2}$ and $|\downarrow\rangle = (|0\rangle-|1\rangle)/\sqrt{2}$ are eigenstates of Pauli operator $\hat{\sigma}^x$]. Moreover, the singlet state is always the Floquet state $|\Phi_1(t)\rangle$ with quasienergy ϵ_1 and independent of the system parameters. In addition, the transition between Floquet states is only allowed in the symmetric subspace. Thus, $\epsilon_{2,3,4}$ together contribute to the Rabi frequency. As shown in Figs. 2(e) and 2(f), the transition frequencies repeatedly appear with period 2ω ($\omega = \Delta$ for the resonant case) due to the interval between different Floquet zones. When $J = 0$, resulting in $\epsilon_2 = 0, \epsilon_3 = -\epsilon_4$, the yellow solid lines, red dotted lines, and blue dashed lines in Fig. 2(e) denote the frequency components characterized by $\epsilon_i - \epsilon_i + 2k\omega$ ($i = 2,3,4$), $\pm\left(\epsilon_2 - \epsilon_{3,4}\right) + 2k\omega$, and $\pm(\epsilon_3 + \omega - \epsilon_4) + 2k\omega$, respectively. However, when $J \neq 0$, the image of transition frequencies becomes more complicated due to the weak-coupling-induced energy shift, especially the splitting between ϵ_1 and ϵ_2. Therefore, transition frequencies derived from the quasienergies give a direct evidence for the numerical results. However, in Figs. 2(c) and 2(d), the bright lines representing the high-frequency components fade away in the weak driving regime, indicating that the fast oscillations can be neglected by RWA.

IV. FULLY ENTANGLED FLOQUET STATE

Note that the avoided crossing of the energy level of the system could cause entanglement resonance of eigenstates in both the time-independent Hamiltonian [74,75] and time-periodic Hamiltonian [76]. Therefore, the sudden splitting of the degenerate energy levels introduced by the weak coupling between flux qubits provides the possibility of Floquet-state entanglement. In the following we turn to the observation of Floquet-state entanglement. The entanglement of the time-dependent Floquet state $|u_r(t)\rangle$ could be characterized by the time-average entanglement over one period T, which is defined as $\bar{\mathcal{C}}_r = 1/T\int_0^T \mathcal{C}[|u_r(t)\rangle]\,dt$ with $\mathcal{C}[|u_r(t)\rangle]$ the instantaneous entanglement of $|u_r(t)\rangle$ [77]. For general state ρ, the entanglement of two qubits can be quantified using the concurrence, which is defined as

$$\mathcal{C} = \max\left\{0, 2\lambda_1 - \sum_{j=1}^{4}\lambda_j\right\}, \tag{10}$$

where $\{\lambda_1,\lambda_2,\lambda_3,\lambda_4\}$ are the square roots of the eigenvalues of $\sqrt{\rho}\left(\hat{\sigma}_y\otimes\hat{\sigma}_y\right)\rho^*\left(\hat{\sigma}_y\otimes\hat{\sigma}_y\right)\sqrt{\rho}$ sorted in a descending order. As we mention in Sec. III, the singlet state $(|\uparrow\downarrow\rangle - |\downarrow\uparrow\rangle)/\sqrt{2}$ in the antisymmetric subspace is the Floquet state $\Phi_1(t)$ with maximally entanglement $\bar{\mathcal{C}}_1 = 1$ all the time. Consequently, we pay attention to the other three Floquet states in the symmetric subspace. For the case of $J = 0$, the Floquet states in the symmetric subspace are $|\Phi_2(t)\rangle = \left[\left|\phi_\uparrow(t)\right\rangle\left|\phi_\downarrow(t)\right\rangle + \left|\phi_\downarrow(t)\right\rangle\left|\phi_\uparrow(t)\right\rangle\right]/\sqrt{2}$, $|\Phi_3(t)\rangle = \left|\phi_\uparrow(t)\right\rangle\left|\phi_\uparrow(t)\right\rangle$ and $|\Phi_4(t)\rangle = \left|\phi_\downarrow(t)\right\rangle\left|\phi_\downarrow(t)\right\rangle$. Here, $\left|\phi_\uparrow(t)\right\rangle = \hat{U}_t|\uparrow\rangle$ and $\left|\phi_\downarrow(t)\right\rangle = \hat{U}_t|\downarrow\rangle$ denote the Floquet states for a single-qubit case with $\hat{U}(t) = \exp\left[-i\int_0^t \Omega\cos\left(\omega t'\right)dt'\hat{\sigma}_z\right]$. Among these Floquet states, $|\Phi_1(t)\rangle$ is always entangled, hence $\bar{\mathcal{C}}_2 = 1$. But $|\Phi_3(t)\rangle$ and $|\Phi_4(t)\rangle$ are separable all the time, resulting in $\bar{\mathcal{C}}_3 = \bar{\mathcal{C}}_4 = 0$. However, when the coupling between two qubits is turned on, the quantum-correlation properties of those Floquet states become complex. As shown in Fig. 3,the entanglement $\bar{\mathcal{C}}_r$ of Floquet state in symmetric subspace is engineered for a wide range of driving parameters $\{\Omega,\omega\}$ and different coupling strengths J. In the weak coupling regime, $\bar{\mathcal{C}}_2$ remains predominantly maximal and $\bar{\mathcal{C}}_{3,4}$ still vanishes in a wide range

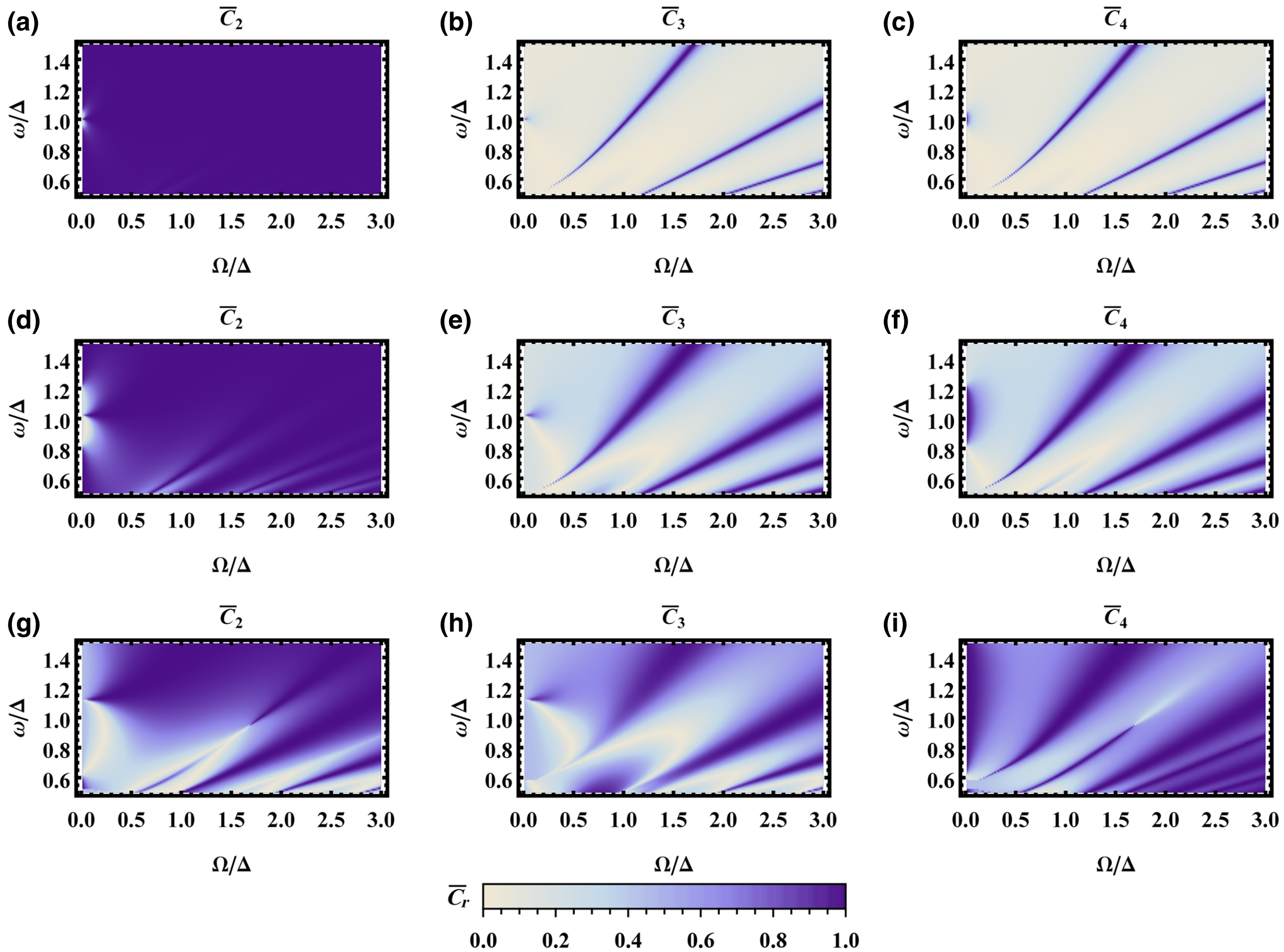

FIG. 3. Density plots describing entanglement $\bar{\mathcal{C}}_r$ of the three symmetric Floquet states in the $\Omega-\omega$ plane for different coupling strengths $J/\Delta=0.05$ in (a)–(c), $J/\Delta=0.2$ in (d)–(f), and $J/\Delta=0.5$ in (g)–(i).

of parameters. Differently, entanglement resonance of $\bar{\mathcal{C}}_{3,4}$ appears in the plane of parameters. When the driving frequency is fixed, multiple choices of driving strength are available for the entanglement resonance. However, compared to the resonant case, the red-detuning driving leads to a wider region with larger driving strength and the blue-detuning driving brings a more narrow region with smaller driving strength. With the coupling strength increasing, the regions representing entanglement resonance are broadened and shifted to overlap eventually, and the feature of entanglement resonance will be weakened and blurred.

To understand the physics behind the entanglement resonance, we investigate the relation between the quasienergy ϵ_r and the entanglement $\bar{\mathcal{C}}_r$ of Floquet state $|\Phi_r(t)\rangle$. As shown in Figs. 4(a) and 4(d),when $J/\Delta\ll 1$, the entanglement $\bar{\mathcal{C}}_r$ is approximate to the noninteracting values. Thus, by sweeping the driving strength, the degeneracy in quasienergy levels of $\Phi_3(t)$ and $\Phi_4(t)$ occurs many times. As shown in Figs. 4(b), 4(e), 4(c), and 4(f), when J/Δ becomes larger, the degenerate levels are separated and the multiple energy crossings are avoided. Note that the points at which the level crossings are avoided match exactly with the one where the entanglement resonance occurs. With the coupling strength increasing, the splitting of the levels are becoming larger, leading to broader entanglement resonances. In addition, one can find that the analytical solution is approaching the numerical one in the limit of $\Omega/\Delta\gg 1$, which is the condition of perturbation approximation. From these results one can conclude that periodic driving modifies the quasienergy levels of two flux qubits and provides an opportunity for energy crossing of the separable Floquet states. Then, the weak coupling between flux qubit separates the degenerate levels and produces avoided crossing, leading to entanglement resonance of the original separable Floquet states.

V. PREPARATION AND DYNAMICS OF ENTANGLEMENT

The entanglement $\bar{\mathcal{C}}_r=1$ requires the concurrence keeping maximal for the whole period $[0,T)$ which implies

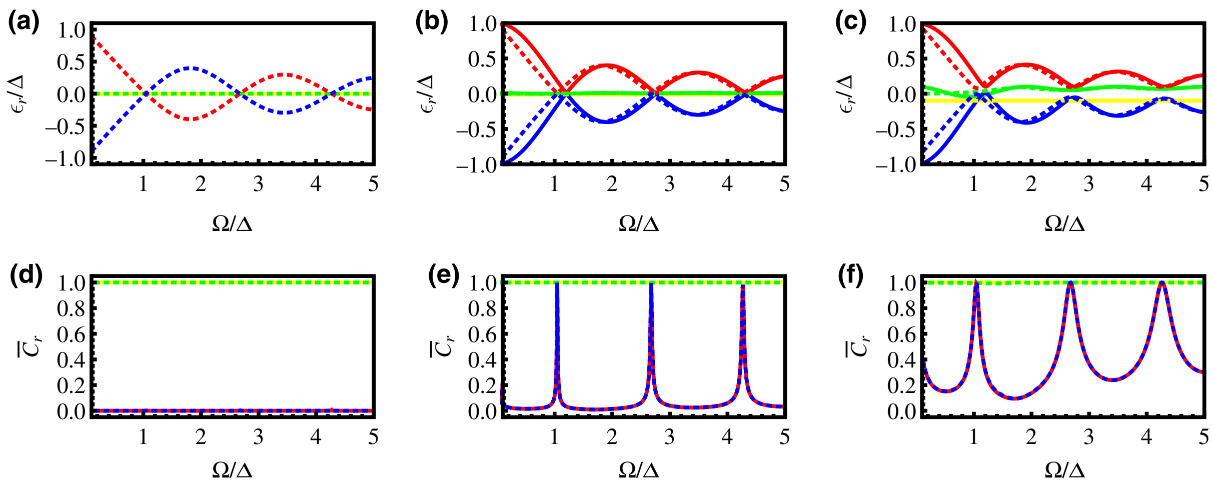

FIG. 4. Quasienergies ϵ_r and entanglement $\bar{\mathcal{C}}_r$ of Floquet states versus resonant driving strength Ω for different coupling strengths $J/\Delta = 0.000\,01$ in (a),(d), $J/\Delta = 0.01$ in (b),(e), and $J/\Delta = 0.1$ in (c),(f), respectively. The dashed lines represent the numerical results and the solid lines represent the analytical results. The yellow, green, red, and blue lines correspond to $r = 1, 2, 3, 4$, respectively.

that the Floquet state $|u_r(t)\rangle$ is maximally entangled all the time. Ideally, if the system is initially prepared into a maximally entangled Floquet state $|u_r(0)\rangle$, its time evolution is described by the wave function $|\Psi(t)\rangle = e^{-i\epsilon_r t}|u_r(t)\rangle$. In this way, the entanglement $\bar{\mathcal{C}}_r = 1$ will be preserved, as the concurrence is independent of the additional exponential factor $e^{-i\epsilon_r t}$.

Before preparing a maximally entangled Floquet state $|u_r(0)\rangle$, three parameters should be traded off to support it. (i) To make sure that the optimal point possesses the maximal entanglement with $\bar{\mathcal{C}}_r = 1$, large coupling strength (still being weak coupling compared to transition frequency) leading to wide peaks of entanglement resonance is favorable for precisely locating the optimal point to obtain the corresponding values of driving parameters. (ii) Although the red-detuning (blue-detuning) driving brings wider (narrower) peaks of entanglement resonance, they play a less significant role than the parameter of coupling strength. Merely, blue-detuning driving is more applicable when the very strong driving cannot be achieved. (iii) When the former two parameters are fixed, driving strength is of many alternatives among the multiple peaks of entanglement resonance. Here we take the maximally entangled Floquet state $|u_r(0)\rangle = \{-0.36 - 0.08i, 0.60, 0.60, 0.35, -0.07i\}$ supported by the set of parameters $\{\Omega/\Delta = 4.26, \omega/\Delta = 1, J/\Delta = 0.05\}$ as an example. Certainly, any other cases are worthy to be considered as long as the maximal entanglement is robust against the tiny fluctuation of the three parameters and the Floquet state is easy to prepare with high fidelity.

The direct coupling between qubits is the most mature method to entangle two flux qubits. Thus, the system for preparing entanglement can be described by a static Hamiltonian

$$\hat{H}_c = \sum_{j=1,2} \frac{\Delta}{2}\hat{\sigma}_j^x + J\hat{\sigma}^z\hat{\sigma}_2^z. \tag{11}$$

Assuming that the coupled system is initialized into the ground state $|\Psi_1(0)\rangle = |11\rangle$, its time evolution $\rho_1(t)$ is governed by an ordinary Markovian master equation in the Schrödinger picture [78,79]

$$\dot{\rho}_1 = -i\left[\hat{H}_c, \rho_1\right] + \mathcal{D}, \tag{12}$$

$$\mathcal{D} = \sum_{j=1,2} \frac{\gamma_j}{2}\left(2\hat{\sigma}_j^-\rho_1\hat{\sigma}_j^+ - \hat{\sigma}_j^+\hat{\sigma}_j^-\rho_1 - \rho_1\hat{\sigma}_j^+\hat{\sigma}_j^-\right), \tag{13}$$

where γ_j and $\hat{\sigma}_j^\pm$ are the dissipation rate and ladder operators of the jth flux qubit. In our simulations, the dissipation rates $\gamma_1/\Delta = \gamma_2/\Delta = 0.001$ are considered for decoherence. Figures 5(a) and 5(b)record the fidelity $\langle u_r(0)|\,\rho_1(t)\,|u_r(0)\rangle$ and the concurrence of $\rho_1(t)$ [77]. At the time $t_d = 33.07/\Delta$, the fidelity reaches the maximum exceeding 95% and concurrence is close to 1. Thus, $\rho_F = \rho_1(t_d)$ can be taken as an approximate Floquet state $|u_r(0)\rangle$.

To protect the entanglement, the technique of Floquet engineering can be applied. Considering decoherence, the time evolution of periodically driven system $\rho_2(t)$ is governed by the Floquet master equation [78,80]

$$\dot{\rho}_2(t) = -i\left[\hat{H}(t), \rho_2(t)\right] + \mathcal{D}(t), \tag{14}$$

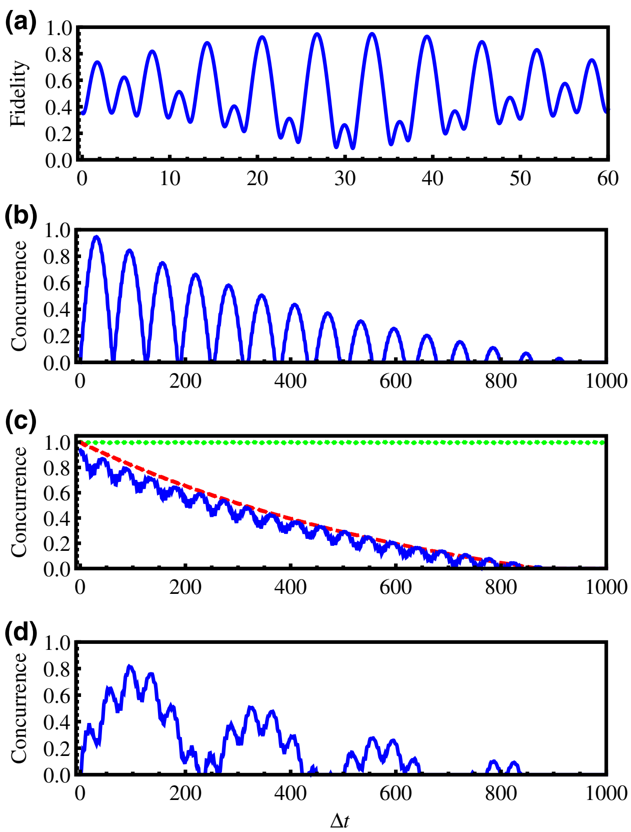

FIG. 5. (a) Fidelity $\langle u_r(0)|\rho_1(t)|u_r(0)\rangle$ and (b) concurrence of $\rho_1(t)$ as a function of Δt with decoherence, where $\Omega = 0, \omega = 0, J/\Delta = 0.05$, and $|\Psi_1(0)\rangle = |11\rangle$. (c) Concurrence of the periodically driven system $\rho_2(t)$ as a function of Δt under different conditions: $|\Psi_2(0)\rangle = |u_r(0)\rangle$ without decoherence (green solid line) and with decoherence (red dashed line), $\rho_2(0) = \rho_F$ with decoherence (blue solid line), where $\Omega/\Delta = 4.26, \omega/\Delta = 1$, and $J/\Delta = 0.05$. (d) Concurrence of the periodically driven system $\rho_2(t)$ as a function of Δt with decoherence, where $|\Psi_2(0)\rangle = |11\rangle$ and $\Omega/\Delta = 4.26, \omega/\Delta = 1$ and $J/\Delta = 0.05$.

$$\mathcal{D}(t) = \sum_{j=1,2}\sum_{\bar{\omega}} \frac{\gamma_j(\bar{\omega})}{2}\Big[2\hat{S}_j(\bar{\omega},t)\rho_2(t)\hat{S}_j^+(\bar{\omega},t) - \hat{S}_j^+(\bar{\omega},t)\hat{S}_j(\bar{\omega},t)\rho_2(t) - \rho_2(t)\hat{S}_j^+(\bar{\omega},t)\hat{S}_j(\bar{\omega},t)\Big], \tag{15}$$

with $\bar{\omega} = \epsilon_{r'} - \epsilon_r - q\omega$. Here, $\hat{S}_j(\bar{\omega},t) = \sum_{r',r,q}\Big[\sum_p \langle\tilde{u}_{r,p}|\hat{\varsigma}_j|\tilde{u}_{r',p+q}\rangle|u_r(t)\rangle\langle u_{r'}(t)|\Big]$ is a part of $\hat{S}_j(t)$ rotating with frequency $\bar{\omega}$, where $\hat{\varsigma}_j = \hat{\sigma}_j^+ + \hat{\sigma}_j^-$ is the Davies operator. $\hat{S}_j^+(\bar{\omega},t)$ is the Hermitian operator for $\hat{S}_j(\bar{\omega},t)$.

In Fig. 5(c), the green solid line has confirmed that the Floquet state $|u_r(t)\rangle$ is maximally entangled all the time for a closed system. However, the Floquet system deviates from the perfect Floquet state by decoherence in an open system, indicated by the red dashed line in Fig. 5(c). When taking ρ_F as the initial state of the Floquet system, the concurrence is imitating the behavior of $|u_r(t)\rangle$ but accompanied by small oscillations caused by the fidelity smaller than 100% [blue solid line in Fig. 5(c)]. However, it is absolutely more stable than the result shown in Fig. 5(b), where the concurrence frequently oscillates to zero before it vanishes due to decoherence. Moreover, for any other states with lower fidelity to the Floquet state $|u_0(t)\rangle$, such as $|11\rangle$ shown in Fig. 5(d), the evolution of entanglement is far from the behavior of the Floquet state $|u_r(t)\rangle$. Longer-time preserved entanglement with smaller oscillation can be expected under the conditions of higher-fidelity state preparation and less decoherence, even approaching to the maximally entangled steady state.

VI. DISCUSSION AND CONCLUSION

We now survey the relevant experimental parameters. All the numerical results are calculated based on the unit of splitting energy $\Delta = 2\pi \times 2.288$ GHz. The driving strength Ω/Δ up to 5 indicates that the amplitude of time-periodic magnetic flux $|\Phi_d| = 5.3\ \mathrm{m}\Phi_0$, and the coupling strength J/Δ varies from 0 to 0.5, yielding that the mutual inductance M ranges from 0 to 1.6 pH [53,81], for the persistent currents $I_p = 690$ nA [69]. The dissipation rate of flux qubit is $\gamma = 2\pi \times 2.288$ MHz in the degeneracy point $\varepsilon = 0$. Additionally, the periodic driving can be approximately realized by high-speed arbitrary waveform generator [69]. Note that the periodic driving technology has been experimentally employed in different systems, such as trapped ions [82], nitrogen-vacancy centers [83], and quantum-dot systems [84,85], and superconducting qubits [69,86–88]. It paves the way to realize our proposed Floquet engineering to generate entanglement between flux qubits via entanglement resonance induced by avoided level crossing.

In conclusion, a pair of superconducting flux qubits driven by a strong periodic microwave field is studied. The periodic driving effectively modifies the Floquet energy spectrum, leading to unprecedented dynamics in the presence of weak coupling between flux qubits. In particular, the maximally entangled state of flux qubits could be realized based on Floquet engineering. Interestingly, the presence of weak coupling between flux qubit lifts the degeneracy of quasienergies and induces the entanglement resonance of the Floquet state. Our scheme lifts greatly the experimental difficulty in changing the static parameters of the system to establish entanglement. This offers our scheme an attractive perspective in the application of quantum-information processing. Floquet engineering is not only an effective method for quantum control but also a wealth of nontrivial quantum phenomena, especially in a many-body quantum system [12]. For instance, to investigate the Floquet-based scheme for quantum simulation in flux-qubit lattices is an interesting topic.

ACKNOWLEDGMENTS

This work is supported by the Hubei Province Science Fund for Distinguished Young Scholars under Grant No. 2020CFA078 and the Youth Innovation Promotion Association (CAS No. 2016299). J.-B.Y. acknowledges support from the National Research Foundation Singapore (Grant No. NRF2017-NRF-NSFC002-015) and No. A*STAR SERC (Grant No. A1685b0005). J.K.X. is supported by Scientific and Technological Research Projects of Hubei provincial department of education B2019070.

APPENDIX A: ANALYTICAL SOLUTIONS OF THE FLOQUET EQUATION

According to the Fourier transform, the time-periodic Floquet state $|u_r(t)\rangle$ can be expanded by a complete set of basis vectors $\{e^{ik\omega t}|k\in\mathbb{Z}\}$ in the temporal space as

$$|u_r(t)\rangle = \sum_k \left|\tilde{u}_{r,k}\right\rangle e^{ik\omega t}, \tag{A1}$$

with $\left|\tilde{u}_{r,k}\right\rangle = 1/T\int_0^T |u_r(t)\rangle\, e^{-ik\omega t}dt$. By substituting Eq. (A1) into the Floquet equation, one can obtain

$$\sum_{k\in\mathbb{Z}}\left[\hat{H}_0^{(k)}\left|\tilde{u}_{r,k}\right\rangle + \hat{H}_1\left|\tilde{u}_{r,k-1}\right\rangle + \hat{H}_1\left|\tilde{u}_{r,k+1}\right\rangle\right]e^{ik\omega t} = \sum_{k\in\mathbb{Z}}\epsilon_r\left|\tilde{u}_{r,k}\right\rangle e^{ik\omega t}. \tag{A2}$$

with $\hat{H}_0^{(k)} = \sum_{i=1,2}(\Delta/2)\,\hat{\sigma}_i^x + J\hat{\sigma}_1^z\hat{\sigma}_2^z + k\omega$, $\hat{H}_1 = \sum_{i=1,2}(\Omega/2)\,\hat{\sigma}_i^z$. Furthermore, a set of equations can be extracted from Eq. (A2) by mapping to different basis vectors $e^{ik\omega t}$, and eventually come down to one tensor equation as

$$\hat{H}_F\left|\tilde{u}_r\right\rangle = \epsilon_r\left|\tilde{u}_r\right\rangle, \tag{A3}$$

with

$$\left|\tilde{u}_r\right\rangle = \left(\cdots\ \left|\tilde{u}_{r,k-1}\right\rangle\ \left|\tilde{u}_{r,k}\right\rangle\ \left|\tilde{u}_{r,k+1}\right\rangle\ \cdots\right)^T \tag{A4}$$

and

$$\hat{H}_F = \begin{pmatrix} \ddots & & & & & & \\ & \hat{H}_0^{(-2)} & \hat{H}_1 & 0 & 0 & 0 & \\ & \hat{H}_1 & \hat{H}_0^{(-1)} & \hat{H}_1 & 0 & 0 & \\ & 0 & \hat{H}_1 & \hat{H}_0^{(0)} & \hat{H}_1 & 0 & \\ & 0 & 0 & \hat{H}_1 & \hat{H}_0^{(1)} & \hat{H}_1 & \\ & 0 & 0 & 0 & \hat{H}_1 & \hat{H}_0^{(2)} & \\ & & & & & & \ddots \end{pmatrix}, \tag{A5}$$

By introducing a perturbation parameter $\lambda = \Delta/2$ ($\Delta \ll \Omega$), the Floquet matrix can be divided into unperturbed and perturbation parts as

$$\hat{H}_F = \hat{H}_0 + \lambda\hat{V}. \tag{A6}$$

The aim is to reduce the infinite-dimensional Floquet matrix $\hat{H}_F$ into the 4×4 effective matrix $\hat{\mathbf{h}}$ using the generalized Van Vleck nearly degenerate perturbation theory [72,73].

In the Sambe space, the unperturbed Hamiltonian

$$\hat{H}_0 = \left(\begin{array}{c|cccc|cccc|cccc|c} \ddots & & & & & & & & & & & & & \\ \hline & J-\omega & 0 & 0 & 0 & \Omega & 0 & 0 & 0 & 0 & 0 & 0 & 0 & \\ & 0 & -J-\omega & 0 & 0 & 0 & 0 & 0 & 0 & 0 & 0 & 0 & 0 & \\ & 0 & 0 & -J-\omega & 0 & 0 & 0 & 0 & 0 & 0 & 0 & 0 & 0 & \\ & 0 & 0 & 0 & J-\omega & 0 & 0 & 0 & -\Omega & 0 & 0 & 0 & 0 & \\ \hline & \Omega & 0 & 0 & 0 & J & 0 & 0 & 0 & \Omega & 0 & 0 & 0 & \\ & 0 & 0 & 0 & 0 & 0 & -J & 0 & 0 & 0 & 0 & 0 & 0 & \\ & 0 & 0 & 0 & 0 & 0 & 0 & -J & 0 & 0 & 0 & 0 & 0 & \\ & 0 & 0 & 0 & -\Omega & 0 & 0 & 0 & J & 0 & 0 & 0 & -\Omega & \\ \hline & 0 & 0 & 0 & 0 & \Omega & 0 & 0 & 0 & J+\omega & 0 & 0 & 0 & \\ & 0 & 0 & 0 & 0 & 0 & 0 & 0 & 0 & 0 & -J+\omega & 0 & 0 & \\ & 0 & 0 & 0 & 0 & 0 & 0 & 0 & 0 & 0 & 0 & -J+\omega & 0 & \\ & 0 & 0 & 0 & 0 & 0 & 0 & 0 & -\Omega & 0 & 0 & 0 & J+\omega & \\ \hline & & & & & & & & & & & & & \ddots \end{array}\right) \tag{A7}$$

is a sparse matrix with all off diagonals being zero in each 4×4 block, indicating that the states $|\Sigma_1\rangle$, $|\Sigma_2\rangle$, $|\Sigma_3\rangle$, and $|\Sigma_4\rangle$ are decoupled from each other. Thus it can be reduced into each one of the four invariant subspaces, resulting in

$$\hat{H}_{0,|\Sigma_i\rangle} = \begin{pmatrix} \ddots & & & & & & \\ & b-2\omega & a & 0 & 0 & 0 & \\ & a & b-\omega & a & 0 & 0 & \\ & 0 & a & b & a & 0 & \\ & 0 & 0 & a & b+\omega & a & \\ & 0 & 0 & 0 & a & b+2\omega & \\ & & & & & & \ddots \end{pmatrix} \tag{A8}$$

with $i = 1, 2, 3, 4$, where $b = J$ and $a = \Omega$ for $i = 1$, $b = -J$ and $a = 0$ for $i = 2, 3$, $b = J$ and $a = -\Omega$ for $i = 4$. If and only if the reduced Hamiltonian $\hat{H}_{0,|\Sigma_i\rangle}$ is all diagonalized, the unperturbed Hamiltonian $\hat{H}_0$ is diagonalized. In each subspace, it can be verified that $\hat{H}_{0,|\Sigma_i\rangle}$ can also result from mapping a function $b + 2a\cos(\omega t) - i(\partial/\partial t)$ into the basis vectors $\left\{e^{ik\omega t} | k \in \mathbb{Z}\right\}$. The reasonable solutions of

$$\left[b + 2a\cos(\omega t) - i\frac{\partial}{\partial t}\right]\mu(t) = \upsilon\mu(t), \tag{A9}$$

are $\upsilon_n = b + n\omega$, correspondingly

$$\mu_n(t) = e^{in\omega t - i(2a/\omega)\sin(\omega t)} = \sum_{k\in\mathbb{Z}} \mathcal{J}_{k-n}\left(-\frac{2a}{\omega}\right) e^{ik\omega t}, \tag{A10}$$

with $n = 0, \pm 1, \pm 2, \ldots$, where the Fourier transform is done and $\mathcal{J}_{k-n}(-2a/\omega)$ is the Bessel function. Consequently, the unperturbed Hamiltonian $\hat{H}_0$ can be diagonalized by

$$\left\{\left|\Phi_{n,1}\right\rangle \left|\Phi_{n,2}\right\rangle \left|\Phi_{n,3}\right\rangle \left|\Phi_{n,4}\right\rangle\right\}, \tag{A11}$$

where

$$\left|\Phi_{n,1}\right\rangle = \sum_{k\in\mathbb{Z}} \mathcal{J}_{k-n}\left(-\frac{2\Omega}{\omega}\right) e^{ik\omega t} |\Sigma_1\rangle, \tag{A12}$$

$$\left|\Phi_{n,2}\right\rangle = e^{in\omega t} |\Sigma_2\rangle, \tag{A13}$$

$$\left|\Phi_{n,3}\right\rangle = e^{in\omega t} |\Sigma_3\rangle, \tag{A14}$$

$$\left|\Phi_{n,4}\right\rangle = \sum_{k\in\mathbb{Z}} \mathcal{J}_{k-n}\left(\frac{2\Omega}{\omega}\right) e^{ik\omega t} |\Sigma_4\rangle. \tag{A15}$$

Taking the eigenstates of $\hat{H}_0$ as the new basis vectors of the Sambe space, the Floquet matrix $\hat{H}_F$ turns to be

$$\hat{H}'_F = \hat{H}'_0 + \lambda\hat{V}', \tag{A16}$$

$$\hat{H}'_0 = \left(\begin{array}{c|cccc|cccc|cccc|c}
\ddots & & & & & & & & & & & & & \\ \hline
 & J-\omega & 0 & 0 & 0 & 0 & 0 & 0 & 0 & 0 & 0 & 0 & 0 & \\
 & 0 & -J-\omega & 0 & 0 & 0 & 0 & 0 & 0 & 0 & 0 & 0 & 0 & \\
 & 0 & 0 & -J-\omega & 0 & 0 & 0 & 0 & 0 & 0 & 0 & 0 & 0 & \\
 & 0 & 0 & 0 & J-\omega & 0 & 0 & 0 & 0 & 0 & 0 & 0 & 0 & \\ \hline
 & 0 & 0 & 0 & 0 & J & 0 & 0 & 0 & 0 & 0 & 0 & 0 & \\
 & 0 & 0 & 0 & 0 & 0 & -J & 0 & 0 & 0 & 0 & 0 & 0 & \\
 & 0 & 0 & 0 & 0 & 0 & 0 & -J & 0 & 0 & 0 & 0 & 0 & \\
 & 0 & 0 & 0 & 0 & 0 & 0 & 0 & J & 0 & 0 & 0 & 0 & \\ \hline
 & 0 & 0 & 0 & 0 & 0 & 0 & 0 & 0 & J+\omega & 0 & 0 & 0 & \\
 & 0 & 0 & 0 & 0 & 0 & 0 & 0 & 0 & 0 & -J+\omega & 0 & 0 & \\
 & 0 & 0 & 0 & 0 & 0 & 0 & 0 & 0 & 0 & 0 & -J+\omega & 0 & \\
 & 0 & 0 & 0 & 0 & 0 & 0 & 0 & 0 & 0 & 0 & 0 & J+\omega & \\ \hline
 & & & & & & & & & & & & & \ddots
\end{array}\right), \tag{A17}$$

$$
\hat{V}' = \left(\begin{array}{c|cccc|cccc|cccc|c}
\ddots & & & & & & & & & & & & & \\
\hline
 & 0 & \tilde{\mathcal{J}}_0 & \tilde{\mathcal{J}}_0 & 0 & 0 & \tilde{\mathcal{J}}_{-1} & \tilde{\mathcal{J}}_{-1} & 0 & 0 & \tilde{\mathcal{J}}_{-2} & \tilde{\mathcal{J}}_{-2} & 0 & \\
 & \tilde{\mathcal{J}}_0 & 0 & 0 & \tilde{\mathcal{J}}_0 & \tilde{\mathcal{J}}_1 & 0 & 0 & \tilde{\mathcal{J}}_{-1} & \tilde{\mathcal{J}}_2 & 0 & 0 & \tilde{\mathcal{J}}_{-2} & \\
 & \tilde{\mathcal{J}}_0 & 0 & 0 & \tilde{\mathcal{J}}_0 & \tilde{\mathcal{J}}_1 & 0 & 0 & \tilde{\mathcal{J}}_{-1} & \tilde{\mathcal{J}}_2 & 0 & 0 & \tilde{\mathcal{J}}_{-2} & \\
 & 0 & \tilde{\mathcal{J}}_0 & \tilde{\mathcal{J}}_0 & 0 & 0 & \tilde{\mathcal{J}}_1 & \tilde{\mathcal{J}}_1 & 0 & 0 & \tilde{\mathcal{J}}_2 & \tilde{\mathcal{J}}_2 & 0 & \\
\hline
 & 0 & \tilde{\mathcal{J}}_1 & \tilde{\mathcal{J}}_1 & 0 & 0 & \tilde{\mathcal{J}}_0 & \tilde{\mathcal{J}}_0 & 0 & 0 & \tilde{\mathcal{J}}_{-1} & \tilde{\mathcal{J}}_{-1} & 0 & \\
 & \tilde{\mathcal{J}}_{-1} & 0 & 0 & \tilde{\mathcal{J}}_1 & \tilde{\mathcal{J}}_0 & 0 & 0 & \tilde{\mathcal{J}}_0 & \tilde{\mathcal{J}}_1 & 0 & 0 & \tilde{\mathcal{J}}_{-1} & \\
 & \tilde{\mathcal{J}}_{-1} & 0 & 0 & \tilde{\mathcal{J}}_1 & \tilde{\mathcal{J}}_0 & 0 & 0 & \tilde{\mathcal{J}}_0 & \tilde{\mathcal{J}}_1 & 0 & 0 & \tilde{\mathcal{J}}_{-1} & \\
 & 0 & \tilde{\mathcal{J}}_{-1} & \tilde{\mathcal{J}}_{-1} & 0 & 0 & \tilde{\mathcal{J}}_0 & \tilde{\mathcal{J}}_0 & 0 & 0 & \tilde{\mathcal{J}}_1 & \tilde{\mathcal{J}}_1 & 0 & \\
\hline
 & 0 & \tilde{\mathcal{J}}_2 & \tilde{\mathcal{J}}_2 & 0 & 0 & \tilde{\mathcal{J}}_1 & \tilde{\mathcal{J}}_1 & 0 & 0 & \tilde{\mathcal{J}}_0 & \tilde{\mathcal{J}}_0 & 0 & \\
 & \tilde{\mathcal{J}}_{-2} & 0 & 0 & \tilde{\mathcal{J}}_2 & \tilde{\mathcal{J}}_{-1} & 0 & 0 & \tilde{\mathcal{J}}_1 & \tilde{\mathcal{J}}_0 & 0 & 0 & \tilde{\mathcal{J}}_0 & \\
 & \tilde{\mathcal{J}}_{-2} & 0 & 0 & \tilde{\mathcal{J}}_2 & \tilde{\mathcal{J}}_{-1} & 0 & 0 & \tilde{\mathcal{J}}_1 & \tilde{\mathcal{J}}_0 & 0 & 0 & \tilde{\mathcal{J}}_0 & \\
 & 0 & \tilde{\mathcal{J}}_{-2} & \tilde{\mathcal{J}}_{-2} & 0 & 0 & \tilde{\mathcal{J}}_{-1} & \tilde{\mathcal{J}}_{-1} & 0 & 0 & \tilde{\mathcal{J}}_0 & \tilde{\mathcal{J}}_0 & 0 & \\
\hline
 & & & & & & & & & & & & & \ddots
\end{array}\right), \tag{A18}
$$

with $\tilde{\mathcal{J}}_n = \mathcal{J}_n(2\Omega/\omega)$, where the properties of Bessel function, such as $\mathcal{J}_n(z) = \mathcal{J}_{-n}(-z)$, $\mathcal{J}_n(y+z) = \sum_m \mathcal{J}_m(y)\,\mathcal{J}_{n-m}(z)$, $\mathcal{J}_{n-1}(z) + \mathcal{J}_{n+1}(z) = (2n/z)\mathcal{J}_n(z)$, and $\sum_m \mathcal{J}_m(z)\,\mathcal{J}_{m-n}(z) = \sum_m \mathcal{J}_m(z)\,\mathcal{J}_{-m+n}(-z) = \mathcal{J}_n(0) = \delta_{n0}$, are utilized.

From the matrix structure of $\hat{H}_F'$, one can identify that the states $\left|\Phi_{0,1(4)}\right\rangle$ are coupled to $\left|\Phi_{n,2(3)}\right\rangle$ throughout the off-diagonal terms $(\Delta/2)\tilde{\mathcal{J}}_n$. When $\left|\Phi_{0,1(4)}\right\rangle$ and $\left|\Phi_{n,2(3)}\right\rangle$ are generated, then the 4×4 effective matrix $\hat{\mathbf{h}}$ can be obtained by neglecting all other coupling terms except the ones between $\left|\Phi_{0,1(4)}\right\rangle$ and $\left|\Phi_{n,2(3)}\right\rangle$. According to the perturbation theory, $\hat{\mathbf{h}}$ and its eigenstates $\boldsymbol{\phi}_i$ can be expanded in powers of λ as

$$
\hat{\mathbf{h}} = \sum_{m=0}^{\infty} \lambda^m \hat{\mathbf{h}}^{(m)}, \tag{A19}
$$

$$
\boldsymbol{\phi}_i = \sum_{m=0}^{\infty} \lambda^m \boldsymbol{\phi}_i^{(m)}, \tag{A20}
$$

with $i = 1,2,3,4$. For n-photon resonance, the expected values of $\hat{H}_F'$ in states $\left|\Phi_{0,1(4)}\right\rangle$, $\left|\Phi_{n,2(3)}\right\rangle$ are nearly degenerate when the condition $J \approx -J + n\omega$ is satisfied. In this situation, the zeroth-order eigenstates are given by

$$
\boldsymbol{\phi}_{1(4)}^{(0)} = \left|\Phi_{0,1(4)}\right\rangle, \tag{A21}
$$

$$
\boldsymbol{\phi}_{2(3)}^{(0)} = \left|\Phi_{n,2(3)}\right\rangle, \tag{A22}
$$

and the zeroth-order matrix $\hat{\mathbf{h}}^{(0)}$ is represented by

$$
\hat{\mathbf{h}}^{(0)} = \begin{pmatrix} J & 0 & 0 & 0 \\ 0 & -J+n\omega & 0 & 0 \\ 0 & 0 & -J+n\omega & 0 \\ 0 & 0 & 0 & J \end{pmatrix}. \tag{A23}
$$

Following the GVV method, a few high-order terms can be obtained as

$$
\boldsymbol{\phi}_1^{(1)} = \sum_{k\neq -n} \frac{\tilde{\mathcal{J}}_k}{2J+k\omega}\left(\left|\Phi_{-k,2}\right\rangle + \left|\Phi_{-k,3}\right\rangle\right), \tag{A24}
$$

$$
\boldsymbol{\phi}_2^{(1)} = \sum_{k\neq -n} \frac{-1}{2J+k\omega}\left[\tilde{\mathcal{J}}_k\left|\Phi_{k+n,1}\right\rangle + \tilde{\mathcal{J}}_{-k}\left|\Phi_{k+n,4}\right\rangle\right], \tag{A25}
$$

$$
\boldsymbol{\phi}_3^{(1)} = \sum_{k\neq -n} \frac{-1}{2J+k\omega}\left[\tilde{\mathcal{J}}_k\left|\Phi_{k+n,1}\right\rangle + \tilde{\mathcal{J}}_{-k}\left|\Phi_{k+n,4}\right\rangle\right], \tag{A26}
$$

$$
\boldsymbol{\phi}_4^{(1)} = \sum_{k\neq -n} \frac{\tilde{\mathcal{J}}_{-k}}{2J+k\omega}\left(\left|\Phi_{-k,2}\right\rangle + \left|\Phi_{-k,3}\right\rangle\right). \tag{A27}
$$

$$
\hat{\mathbf{h}}^{(1)} = \begin{pmatrix} 0 & \tilde{\mathcal{J}}_{-n} & \tilde{\mathcal{J}}_{-n} & 0 \\ \tilde{\mathcal{J}}_{-n} & 0 & 0 & \tilde{\mathcal{J}}_n \\ \tilde{\mathcal{J}}_{-n} & 0 & 0 & \tilde{\mathcal{J}}_n \\ 0 & \tilde{\mathcal{J}}_n & \tilde{\mathcal{J}}_n & 0 \end{pmatrix}, \tag{A28}
$$

$$\hat{\mathbf{h}}^{(2)} = \sum_{k\neq -n} \frac{1}{2J+k\omega} \begin{pmatrix} 2\tilde{\mathcal{J}}_k^2 & 0 & 0 & 2\tilde{\mathcal{J}}_{-k}\tilde{\mathcal{J}}_k \\ 0 & -\left[\tilde{\mathcal{J}}_k^2+\tilde{\mathcal{J}}_{-k}^2\right] & -\left[\tilde{\mathcal{J}}_k^2+\tilde{\mathcal{J}}_{-k}^2\right] & 0 \\ 0 & -\left[\tilde{\mathcal{J}}_k^2+\tilde{\mathcal{J}}_{-k}^2\right] & -\left[\tilde{\mathcal{J}}_k^2+\tilde{\mathcal{J}}_{-k}^2\right] & 0 \\ 2\tilde{\mathcal{J}}_{-k}\tilde{\mathcal{J}}_k & 0 & 0 & 2\tilde{\mathcal{J}}_{-k}^2 \end{pmatrix}, \tag{A29}$$

$$\hat{\mathbf{h}}^{(3)} = \sum_{k\neq -n} \left(\sum_{l\neq -n} \frac{-2\left[\tilde{\mathcal{J}}_l\tilde{\mathcal{J}}_{k+l+n}+\tilde{\mathcal{J}}_{-l}\tilde{\mathcal{J}}_{-(k+l+n)}\right]}{(2J+k\omega)(2J+l\omega)} \right) \begin{pmatrix} 0 & \tilde{\mathcal{J}}_k & \tilde{\mathcal{J}}_k & 0 \\ \tilde{\mathcal{J}}_k & 0 & 0 & \tilde{\mathcal{J}}_{-k} \\ \tilde{\mathcal{J}}_k & 0 & 0 & \tilde{\mathcal{J}}_{-k} \\ 0 & \tilde{\mathcal{J}}_{-k} & \tilde{\mathcal{J}}_{-k} & 0 \end{pmatrix}. \tag{A30}$$

Finally, the infinite-dimensional $\hat{H}_F'$ is reduced into a 4×4 effective matrix

$$\hat{\mathbf{h}} = \sum_{k\neq -n} \begin{pmatrix} J+\frac{\eta_k}{2}\Delta^2\tilde{\mathcal{J}}_k^2 & \frac{1}{2}\Delta\tilde{\mathcal{J}}_{-n}-\frac{\xi_k}{4}\Delta^3\tilde{\mathcal{J}}_k & \frac{1}{2}\Delta\tilde{\mathcal{J}}_{-n}-\frac{\xi_k}{4}\Delta^3\tilde{\mathcal{J}}_k & \frac{\eta_k}{2}\Delta^2\tilde{\mathcal{J}}_{-k}\tilde{\mathcal{J}}_k \\ \frac{1}{2}\Delta\tilde{\mathcal{J}}_{-n}-\frac{\xi_k}{4}\Delta^3\tilde{\mathcal{J}}_k & -J+n\omega-\frac{\eta_k}{4}\Delta^2\left[\tilde{\mathcal{J}}_k^2+\tilde{\mathcal{J}}_{-k}^2\right] & -\frac{\eta_k}{4}\Delta^2\left[\tilde{\mathcal{J}}_k^2+\tilde{\mathcal{J}}_{-k}^2\right] & \frac{1}{2}\Delta\tilde{\mathcal{J}}_n-\frac{\xi_k}{4}\Delta_k^3\tilde{\mathcal{J}}_{-k} \\ \frac{1}{2}\Delta\tilde{\mathcal{J}}_{-n}-\frac{\xi_k}{4}\Delta^3\tilde{\mathcal{J}}_k & -\frac{\eta_k}{4}\Delta^2\left[\tilde{\mathcal{J}}_k^2+\tilde{\mathcal{J}}_{-k}^2\right] & -J+n\omega-\frac{\eta_k}{4}\Delta^2\left[\tilde{\mathcal{J}}_k^2+\tilde{\mathcal{J}}_{-k}^2\right] & \frac{1}{2}\Delta\tilde{\mathcal{J}}_n-\frac{\xi_k}{4}\Delta^3\tilde{\mathcal{J}}_{-k} \\ \frac{\eta_k}{2}\Delta^2\tilde{\mathcal{J}}_{-k}\tilde{\mathcal{J}}_k & \frac{1}{2}\Delta\tilde{\mathcal{J}}_n-\frac{\xi_k}{4}\Delta^3\tilde{\mathcal{J}}_{-k} & \frac{1}{2}\Delta\tilde{\mathcal{J}}_n-\frac{\xi_k}{4}\Delta^3\tilde{\mathcal{J}}_{-k} & J+\frac{\eta_k}{2}\Delta^2\tilde{\mathcal{J}}_{-k}^2 \end{pmatrix}, \tag{A31}$$

with

$$\eta_k = \frac{1}{2J+k\omega}, \tag{A32}$$

$$\xi_k = \sum_{l\neq -n} \frac{\tilde{\mathcal{J}}_l\tilde{\mathcal{J}}_{k+l+n}+\tilde{\mathcal{J}}_{-l}\tilde{\mathcal{J}}_{-(k+l+n)}}{(2J+k\omega)(2J+l\omega)}. \tag{A33}$$

Therefore the four quasi-energies in one Floquet zone can be obtain by diagonalizing the 4×4 effective Hamiltonian.

In the weak coupling limit, i.e., $J \ll \omega$, the near degenerate condition $J \approx -J + n\omega$ can be satisfied by $n = 0$. After neglecting Δ^3 terms and $\eta_{|k|\geq 2}$ terms, the effective Hamiltonian is simplied to

$$\hat{H}_{\mathrm{GVV}} = \begin{pmatrix} J+\varkappa\Delta^2\tilde{\mathcal{J}}_1^2 & \frac{1}{2}\Delta\tilde{\mathcal{J}}_0 & \frac{1}{2}\Delta\tilde{\mathcal{J}}_0 & -\varkappa\Delta^2\tilde{\mathcal{J}}_1^2 \\ \frac{1}{2}\Delta\tilde{\mathcal{J}}_0 & -J-\varkappa\Delta^2\tilde{\mathcal{J}}_1^2 & -\varkappa\Delta^2\tilde{\mathcal{J}}_1^2 & \frac{1}{2}\Delta\tilde{\mathcal{J}}_0 \\ \frac{1}{2}\Delta\tilde{\mathcal{J}}_0 & -\varkappa\Delta^2\tilde{\mathcal{J}}_1^2 & -J-\varkappa\Delta^2\tilde{\mathcal{J}}_1^2 & \frac{1}{2}\Delta\tilde{\mathcal{J}}_0 \\ -\varkappa\Delta^2\tilde{\mathcal{J}}_1^2 & \frac{1}{2}\Delta\tilde{\mathcal{J}}_0 & \frac{1}{2}\Delta\tilde{\mathcal{J}}_0 & J+\varkappa\Delta^2\tilde{\mathcal{J}}_1^2 \end{pmatrix}, \tag{A34}$$

with $\varkappa = 2J/(4J^2-\omega^2)$, where the property of Bessel function $J_{-k}(z) = (-1)^k J_k(z)$ is used. And the four quasienergies are

$$\epsilon_1 = -J, \tag{A35}$$

$$\epsilon_2 = J + 2\varkappa\Delta^2\tilde{\mathcal{J}}_1^2, \tag{A36}$$

$$\epsilon_3 = -\varkappa\Delta^2\tilde{\mathcal{J}}_1^2 - \sqrt{\Delta^2\tilde{\mathcal{J}}_0^2 + \left(J+\varkappa\Delta^2\tilde{\mathcal{J}}_1^2\right)^2}, \tag{A37}$$

$$\epsilon_4 = -\varkappa\Delta^2\tilde{\mathcal{J}}_1^2 + \sqrt{\Delta^2\tilde{\mathcal{J}}_0^2 + \left(J + \varkappa\Delta^2\tilde{\mathcal{J}}_1^2\right)^2}. \quad \text{(A38)}$$

[1] J. E. Lang, R. B. Liu, and T. S. Monteiro, Dynamical-Decoupling-Based Quantum Sensing: Floquet Spectroscopy, Phys. Rev. X **5**, 041016 (2015).
[2] F. Grossmann, T. Dittrich, P. Jung, and P. Hänggi, Coherent Destruction of Tunneling, Phys. Rev. Lett. **67**, 516 (1991).
[3] C. Navarrete-Benlloch, J. J. García-Ripoll, and D. Porras, Inducing Nonclassical Lasing via Periodic Drivings in Circuit Quantum Electrodynamics, Phys. Rev. Lett. **113**, 193601 (2014).
[4] H. Lignier, C. Sias, D. Ciampini, Y. Singh, A. Zenesini, O. Morsch, and E. Arimondo, Dynamical Control of Matter-Wave Tunneling in Periodic Potentials, Phys. Rev. Lett. **99**, 220403 (2007).
[5] C. Chen, J.-H. An, H.-G. Luo, C. P. Sun, and C. H. Oh, Floquet control of quantum dissipation in spin chains, Phys. Rev. A **91**, 052122 (2015).
[6] D. Vorberg, W. Wustmann, R. Ketzmerick, and A. Eckardt, Generalized Bose-Einstein Condensation into Multiple States in Driven-Dissipative Systems, Phys. Rev. Lett. **111**, 240405 (2013).
[7] P. Hauke, O. Tieleman, A. Celi, C. Ölschläger, J. Simonet, J. Struck, M. Weinberg, P. Windpassinger, K. Sengstock, M. Lewenstein, and A. Eckardt, Non-Abelian Gauge Fields and Topological Insulators in Shaken Optical Lattices, Phys. Rev. Lett. **109**, 145301 (2012).
[8] N. H. Lindner, G. Refael, and V. Galitski, Floquet topological insulator in semiconductor quantum wells, Nat. Phys. **7**, 490 (2011).
[9] M. C. Rechtsman, J. M. Zeuner, Y. Plotnik, Y. Lumer, S. Nolte, M. Segev, and A. Szameit, Photonic Floquet topological insulators, Nature **496**, 196 (2013).
[10] L. Guo, M. Marthaler, and G. Schön, Phase Space Crystals: A New Way to Create a Quasienergy Band Structure, Phys. Rev. Lett. **111**, 205303 (2013).
[11] S. Basak, Y. Chougale, and R. Nath, Periodically Driven Array of Single Rydberg Atoms, Phys. Rev. Lett. **120**, 123204 (2018).
[12] O. Kyriienko and A. S. Sørensen, Floquet Quantum Simulation with Superconducting Qubits, Phys. Rev. Appl. **9**, 064029 (2018).
[13] A. Colcelli, G. Mussardo, G. Sierra, and A. Trombettoni, Integrable Floquet Hamiltonian for a Periodically Tilted 1D Gas, Phys. Rev. Lett. **123**, 130401 (2019).
[14] P. Ponte, Z. Papić, F. Huveneers, and D. A. Abanin, Many-Body Localization in Periodically Driven Systems, Phys. Rev. Lett. **114**, 140401 (2015).
[15] L. D'Alessio and Marcos Rigol, Long-Time Behavior of Isolated Periodically Driven Interacting Lattice Systems, Phys. Rev. X **4**, 041048 (2014).
[16] N. H. Lindner, E. Berg, and M. S. Rudner, Universal Chiral Quasisteady States in Periodically Driven Many-Body Systems, Phys. Rev. X **7**, 011018 (2017).
[17] A. Russomanno, A. Silva, and G. E. Santoro, Periodic Steady Regime and Interference in a Periodically Driven Quantum System, Phys. Rev. Lett. **109**, 257201 (2012).
[18] H. Landa, M. Schiró, and G. Misguich, Multistability of Driven-Dissipative Quantum Spins, Phys. Rev. Lett. **124**, 043601 (2020).
[19] A. Eckardt, C. Weiss, and M. Holthaus, Superfluid-Insulator Transition in a Periodically Driven Optical Lattice, Phys. Rev. Lett. **95**, 260404 (2005).
[20] T. Prosen and E. Ilievski, Nonequilibrium Phase Transition in a Periodically Driven *XY* Spin Chain, Phys. Rev. Lett. **107**, 060403 (2011).
[21] S. Mathey and S. Diehl, Absence of Criticality in the Phase Transitions of Open Floquet Systems, Phys. Rev. Lett. **122**, 110602 (2019).
[22] D. Carpentier, P. Delplace, M. Fruchart, and K. Gawedzki, Topological Index for Periodically Driven Time-Reversal Invariant 2D Systems, Phys. Rev. Lett. **114**, 106806 (2015).
[23] N. Goldman, J. C. Budich, and P. Zoller, Topological quantum matter with ultracold gases in optical lattices, Nat. Phys. **12**, 639 (2016).
[24] N. Goldman and J. Dalibard, Periodically Driven Quantum Systems: Effective Hamiltonians and Engineered Gauge Fields, Phys. Rev. X **4**, 031027 (2014).
[25] A. C. Potter, T. Morimoto, and A. Vishwanath, Classification of Interacting Topological Floquet Phases in One Dimension, Phys. Rev. X **6**, 041001 (2016).
[26] H. P. Hu, B. Huang, E. Zhao, and W. V. Liu, Dynamical Singularities of Floquet Higher-Order Topological Insulators, Phys. Rev. Lett. **124**, 057001 (2020).
[27] M. S. Rudner, N. H. Lindner, E. Berg, and M. Levin, Anomalous Edge States and the Bulk-Edge Correspondence for Periodically Driven Two-Dimensional Systems, Phys. Rev. X **3**, 031005 (2013).
[28] P. Nevado, S. Fernández-Lorenzo, and D. Porras, Topological Edge States in Periodically Driven Trapped-Ion Chains, Phys. Rev. Lett. **119**, 210401 (2017).
[29] F. Nathan, M. S. Rudner, N. H. Lindner, E. Berg, and G. Refael, Quantized Magnetization Density in Periodically Driven Systems, Phys. Rev. Lett. **119**, 186801 (2017).
[30] Z. J. Shu, Y. Liu, Q. Y. Cao, P. C. Yang, S. L. Zhang, M. B. Plenio, F. Jelezko, and J. M. Cai, Observation of Floquet Raman Transition in a Driven Solid-State Spin System, Phys. Rev. Lett. **121**, 210501 (2018).
[31] K. Ji and B. V. Fine, Suppression of Heating in Quantum Spin Clusters under Periodic Driving as a Dynamic Localization Effect, Phys. Rev. Lett. **121**, 050602 (2018).
[32] O. Howell, P. Weinberg, D. Sels, A. Polkovnikov, and M. Bukov, Asymptotic Prethermalization in Periodically Driven Classical Spin Chains, Phys. Rev. Lett. **122**, 010602 (2019).
[33] C. Kuhlenkamp and M. Knap, Periodically Driven Sachdev-Ye-Kitaev Models, Phys. Rev. Lett. **124**, 106401 (2020).
[34] M. Bukov, M. Kolodrubetz, and A. Polkovnikov, Schrieffer-Wolff Transformation for Periodically Driven Systems: Strongly Correlated Systems with Artificial Gauge Fields, Phys. Rev. Lett. **116**, 125301 (2016).
[35] T. Mori, T. Kuwahara, and K. Saito, Rigorous Bound on Energy Absorption and Generic Relaxation in Periodically Driven Quantum Systems, Phys. Rev. Lett. **116**, 120401 (2016).

[36] D. V. Else, B. Bauer, and C. Nayak, Floquet Time Crystals, Phys. Rev. Lett. **117**, 090402 (2016).
[37] A. K. Eissing, V. Meden, and D. M. Kennes, Renormalization in Periodically Driven Quantum Dots, Phys. Rev. Lett. **116**, 026801 (2016).
[38] A. Das, Exotic freezing of response in a quantum many-body system, Phys. Rev. B **82**, 172402 (2010).
[39] Y. Wu and X. Yang, Strong-Coupling Theory of Periodically Driven Two-Level Systems, Phys. Rev. Lett. **98**, 013601 (2007).
[40] P. Bordia, H. Lüschen, U. Schneider, M. Knap, and I. Block, Periodically driving a many-body localized quantum system, Nat. Phys. **13**, 460 (2017).
[41] S. Choi, J. Choi, R. Landig, G. Kucsko, H. Zhou, J. Isoya, F. Jelezko, S. Onoda, H. Sumiya, V. Khemani, C. von Keyserlingk, N. Y. Yao, E. Demler, and M. D. Lukin, Observation of discrete time-crystalline order in a disordered dipolar many-body system, Nature **543**, 221 (2017).
[42] J. Rovny, R. L. Blum, and S. E. Barrett, Observation of Discrete-Time-Crystal Signatures in an Ordered Dipolar Many-Body System, Phys. Rev. Lett. **120**, 180603 (2018).
[43] S. Pal, N. Nishad, T. S. Mahesh, and G. J. Sreejith, Temporal Order in Periodically Driven Spins in Star-Shaped Clusters, Phys. Rev. Lett. **120**, 180602 (2018).
[44] J. Zhang, P. W. Hess, A. Kyprianidis, P. Becker, A. Lee, J. Smith, G. Pagano, I. D. Potirniche, A. C. Potter, A. Vishwanath, N. Y. Yao, and C. Monroe, Observation of a discrete time crystal, Nature **543**, 217 (2017).
[45] A. Lazarides, A. Das, and R. Moessner, Periodic Thermodynamics of Isolated Quantum Systems, Phys. Rev. Lett. **112**, 150401 (2014).
[46] J. Eisert, M. Friesdorf, and C. Gogolin, Quantum many-body systems out of equilibrium, Nat. Phys. **11**, 124 (2015).
[47] R. Moessner and S. L. Sondhi, Equilibration and order in quantum Floquet matter, Nat. Phys. **13**, 424 (2017).
[48] F. Bloch and A. Siegert, Magnetic resonance for nonrotating fields, Phys. Rev. **57**, 522 (1940).
[49] J. H. Shirley, Solution of the Schrödinger equation with a Hamiltonian periodic in time, Phys. Rev. **138**, B979 (1965).
[50] Y. B. Zeldovich, The quasienergy of a quantum-mechanical system subjected to a periodic action, Sov. Phys. JETP **24**, 1006 (1967).
[51] J. E. Mooij, T. P. Orlando, L. Levitov, L. Tian, C. H. van der Wal, and S. Lloyd, Josephson persistent-current qubit, Science **285**, 1036 (1999).
[52] T. P. Orlando, J. E. Mooij, L. Tian, C. H. van der Wal, L. Levitov, S. Lloyd, and J. J. Mazo, Superconducting persistent-current qubit, Phys. Rev. B **60**, 15398 (1999).
[53] J. B. Majer, F. G. Paauw, A. C. J. ter Haar, C. J. P. M. Harmans, and J. E. Mooij, Spectroscopy on Two Coupled Superconducting Flux Qubits, Phys. Rev. Lett. **94**, 090501 (2005).
[54] C. Rigetti, A. Blais, and M. Devoret, Protocol for Universal Gates in Optimally Biased Superconducting Qubits, Phys. Rev. Lett. **94**, 240502 (2005).
[55] S. Ashhab, S. Matsuo, N. Hatakenaka, and F. Nori, Generalized switchable coupling for superconducting qubits using double resonance, Phys. Rev. B **74**, 184504 (2006).
[56] Y. X. Liu, L. F. Wei, J. S. Tsai, and F. Nori, Controllable Coupling between Flux Qubits, Phys. Rev. Lett. **96**, 067003 (2006).
[57] J. H. Plantenberg, P. C. de Groot, C. J. P. M. Harmans, and J. E. Mooij, Demonstration of controlled-NOT quantum gates on a pair of superconducting quantum bits, Nature **447**, 836 (2007).
[58] J. Majer, J. M. Chow, J. M. Gambetta, J. Koch, B. R. Johnson, J. A. Schreier, L. Frunzio, D. I. Schuster, A. A. Houck, A. Wallraff, A. Blais, M. H. Devoret, S. M. Girvin, and R. J. Schoelkopf, Coupling superconducting qubits via a cavity bus, Nature **449**, 443 (2007).
[59] J. Li, K. Chalapat, and G. S. Paraoanu, Entanglement of superconducting qubits via microwave fields: Classical and quantum regimes, Phys. Rev. B **78**, 064503 (2008).
[60] J. Li and G. S. Paraoanu, Generation and propagation of entanglement in driven coupled-qubit systems, New J. Phys. **11**, 113020 (2009).
[61] P. C. de Groot, J. Lisenfeld, R. N. Schouten, S. Ashhab, A. Lupascu, C. J. P. M. Harmans, and J. E. Mooij, Selective darkening of degenerate transitions demonstrated with two superconducting quantum bits, Nat. Phys. **6**, 763 (2010).
[62] C. Rigetti and M. Devoret, Fully microwave-tunable universal gates in superconducting qubits with linear couplings and fixed transition frequencies, Phys. Rev. B **81**, 134507 (2010).
[63] J. M. Chow, A. D. Córcoles, J. M. Gambetta, C. Rigetti, B. R. Johnson, J. A. Smolin, J. R. Rozen, G. A. Keefe, M. B. Rothwell, M. B. Ketchen, and M. Steffen, Simple All-Microwave Entangling Gate for Fixed-Frequency Superconducting Qubits, Phys. Rev. Lett. **107**, 080502 (2011).
[64] A. M. Stanin, M. V. Denisenko, S. Ashhab, and F. Nori, Amplitude spectroscopy of two coupled qubits, Phys. Rev. B **85**, 184524 (2012).
[65] M. Bal, C. Deng, J.-L. Orgiazzi, F. R. Ong, and A. Lupascu, Ultrasensitive magnetic field detection using a single artificial atom, Nat. Commun. **3**, 1324 (2012).
[66] L. Chakhmakhchyan, C. Leroy, N. Ananikian, and S. Guérin, Ultrasensitive magnetic field detection using a single artificial atom, Phys. Rev. A **90**, 042324 (2014).
[67] A. L. Gramajo, D. Domínguez, and M. J. Sánchez, Entanglement generation through the interplay of harmonic driving and interaction in coupled superconducting qubits, Eur. Phys. J. B **90**, 255 (2017).
[68] A. L. Gramajo, D. Domínguez, and M. J. Sánchez, Amplitude tuning of steady-state entanglement in strongly driven coupled qubits, Phys. Rev. A **98**, 042337 (2018).
[69] C. Q. Deng, J. L. Orgiazzi, F. R. Shen, S. Ashhab, and A. Lupascu, Observation of Floquet States in a Strongly Driven Artificial Atom, Phys. Rev. Lett. **115**, 133601 (2015).
[70] H. Sambe, Steady states and quasienergies of a quantum-mechanical system in an oscillating field, Phys. Rev. A **7**, 2203 (1973).
[71] V. Novičenko, E. Anisimovas, and G. Juzeliūnas, Floquet analysis of a quantum system with modulated periodic driving, Phys. Rev. A **95**, 023615 (2017).
[72] S. K. Son, S. Han, and Shih-I. Chu, Floquet formulation for the investigation of multiphoton quantum interference in a superconducting qubit driven by a strong ac field, Phys. Rev. A **79**, 032301 (2009).

[73] K. Szczygielski, On the application of Floquet theorem in development of time-dependent Lindbladians, J. Math. Phys. **55**, 083506 (2014).

[74] J. Karthik, A. Sharma, and A. Lakshminarayan, On the application of Floquet theorem in development of time-dependent Lindbladians, Phys. Rev. A **75**, 022304 (2007).

[75] D. Bruß, N. Datta, A. Ekert, L. C. Kwek, and C. Macchiavello, Multipartite entanglement in quantum spin chains, Phys. Rev. A **72**, 014301 (2005).

[76] S. Sauer, F. Mintert, C. Gneiting, and A. Buchleitner, Entanglement resonances of driven multi-partite quantum systems, J. Phys. B **45**, 154011 (2012).

[77] W. K. Wootters, Entanglement of Formation of an Arbitrary State of Two Qubits, Phys. Rev. Lett. **80**, 2245 (1998).

[78] H. P. Breuer and F. Petruccione, *The Theory of Open Quantum Systems* (Oxford University Press, Oxford, 2002).

[79] E. B. Davies, Markovian master equations, Commun. Math. Phys. **39**, 91 (1974).

[80] E. B. Davies and H. Spohn, Open quantum systems with time-dependent Hamiltonians and their linear response, J. Stat. Phys. **19**, 511 (1978).

[81] P. M. Billangeon, J. S. Tsai, and Y. Nakamura, Scalable architecture for quantum information processing with superconducting flux qubits based on purely longitudinal interactions, Phys. Rev. B **92**, 020509(R) (2015).

[82] K. Kim, M. S. Chang, S. Korenblit, R. Islam, E. E. Edwards, J. K. Freericks, G. D. Lin, L. M. Duan, and C. Monroe, Quantum simulation of frustrated Ising spins with trapped ions, Nature **465**, 590 (2010).

[83] P. Neumann, R. Kolesov, B. Naydenov, J. Beck, F. Rempp, M. Steiner, V. Jacques, G. Balasubramanian, M. L. Markham, D. J. Twitchen, S. Pezzagna, J. Meijer, J. Twamley, F. Jelezko, and J. Wrachtrup, Quantum register based on coupled electron spins in a room-temperature solid, Nat. Phys. **6**, 249 (2010).

[84] J. V. Koski, A. J. Landig, A. Pályi, P. Scarlino, C. Reichl, W. Wegscheider, G. Burkard, A. Wallraff, K. Ensslin, and T. Ihn, Floquet Spectroscopy of a Strongly Driven Quantum Dot Charge Qubit with a Microwave Resonator, Phys. Rev. Lett. **121**, 043603 (2018).

[85] F. Forster, G. Petersen, S. Manus, P. Hänggi, D. Schuh, W. Wegscheider, S. Kohler, and S. Ludwig, Characterization of Qubit Dephasing by Landau-Zener-Stückelberg-Majorana Interferometry, Phys. Rev. Lett. **112**, 116803 (2014).

[86] P. Y. Wen, A. F. Kockum, H. Ian, J. C. Chen, F. Nori, and I.-C. Hoi, Reflective Amplification without Population Inversion from a Strongly Driven Superconducting Qubit, Phys. Rev. Lett. **120**, 063603 (2018).

[87] R. McDermott, R. W. Simmonds, M. Steffen, K. B. Cooper, K. Cicak, K. D. Osborn, Seongshik Oh, D. P. Pappas, and John M. Martinis, Simultaneous state measurement of coupled Josephson phase qubits, Science **307**, 1299 (2005).

[88] J. Pan, H. Z. Jooya, G. Sun, Y. Fan, P. Wu, D. A. Telnov, Shih-I. Chu, and S. Han, Absorption spectra of superconducting qubits driven by bichromatic microwave fields, Phys. Rev. B **96**, 174518 (2017).